Journal of Marine Science and Technology

Volume 24 | Issue 5 Article 8

APPLICATION OF AN EXTENSION NEURAL NETWORK METHOD FOR FAULT DIAGNOSIS OF THREE-LEVEL INVERTERS USED IN MARINE VESSELS

Kuei-Hsiang Chao
Department of Electrical Engineering, National Chin-Yi University of Technology, Taichung, Taiwan, R.O.C.,
chaokh@ncut.edu.tw

Yu-Ren Shen
Department of Electrical Engineering, National Chin-Yi University of Technology, Taichung, Taiwan, R.O.C

Recommended Citation

Chao, Kuei-Hsiang and Shen, Yu-Ren (2016) "APPLICATION OF AN EXTENSION NEURAL NETWORK METHOD FOR FAULT DIAGNOSIS OF THREE-LEVEL INVERTERS USED IN MARINE VESSELS," *Journal of Marine Science and Technology*: Vol. 24: Iss. 5, Article 8.
DOI: 10.6119/JMST-016-0604-1
Available at: https://jmstt.ntou.edu.tw/journal/vol24/iss5/8

APPLICATION OF AN EXTENSION NEURAL NETWORK METHOD FOR FAULT DIAGNOSIS OF THREE-LEVEL INVERTERS USED IN MARINE VESSELS

Acknowledgements

This work was supported by the Ministry of Science and Technology, Taiwan, under the Grant MOST 103-2221-E167-015-MY3.

Journal of Marine Science and Technology, Vol. 24, No.5, pp. 968-979 (2016)
DOI: 10.6119/JMST-016-0604-1

APPLICATION OF AN EXTENSION NEURAL NETWORK METHOD FOR FAULT DIAGNOSIS OF THREE-LEVEL INVERTERS USED IN MARINE VESSELS

Kuei-Hsiang Chao and Yu-Ren Shen

Key words: extension neural network, fault diagnosis, inverter, characteristics spectrum.

ABSTRACT

This study proposes an extension neural network (ENN) algorithm to carry out the fault diagnosis of an inverter in a motor drive system for marine vessels. First, we use PSIM software to construct a three-level neutral point clamped (NPC) inverter, which simulates the occurrence of the fault of any power transistor in the NPC inverter. Simultaneously, we use fast Fourier transforms to transcribe the waveform of phase voltage in the time domain during the fault of any power transistor entering the spectrum in the frequency domain, looking for the corresponding characteristic spectrum during the fault of the power transistor. Next, we establish the relationship between the fault type and the specific characteristic spectrum as the learning basis of the extension neural network. By doing so, we build up a fault diagnosis system for the inverter. Finally, we use the simulation results to verify the feasibility of the proposed inverter fault diagnosis system.

I. INTRODUCTION

Recently, there has been extensive electrical drive development in marine vessels, which depends on motors for activation. Control of the rotation speed of a motor can be achieved with an inverter, which transforms DC voltage into AC voltage, so rotation speeds of the motor change along with the change of output AC frequency. However, traditional two-level inverters are limited to high voltages and high power field requirements. To overcome this defect, the structure and application of multi-level inverters have been studied (Rodríguez et al., 2002; Rodriguez and Leeb, 2006; Daher et al., 2008). A multi-level inverter consists of several power transistors, which are assembled in serial and in parallel. Generally speaking, if a multi-level inverter has more power transistors, then dv/dt at the output end will be reduced, and the waveform of the output voltage will become closer to a sinusoidal waveform. Then the power rating and voltage rating of power transistors can be reduced to extend their effective life cycle. There are other advantages as well, such as reducing harmonics, decreasing energy loss and improving electromagnetic interference (EMI). Thus the circuit structure of multi-level inverters has been widely applied in many areas. However, multi-level inverters also have some defects. For instance, with more levels there is more power transistors needed, which raises the costs of circuits and makes it more difficult to control. Due to this factor, multi-level inverters are more likely to be faulty during operation, and so the fault diagnosis of inverters has become an important research issue.

The application of artificial intelligence (AI) based techniques can be advantageous in fault diagnosis since these diagnoses have several advantages. For instance, since AI-based techniques do not require mathematical models, the development time can be significantly reduced. A literature review of recent developments in the field of AI-based diagnostic systems in power inverters has been presented (Lu and Sharma, 2009). In addition, some scholars have studied the application of a neural network (NN) to establish a fault diagnosis system and judge the faults of power transistors (Ju et al., 2006; Khomfoi and Tolbert, 2007). These NN-based fault diagnosis methods allow an accurate solution to a particular fault problem without accurate knowledge of the faulty system. However, their main drawback is due to the fact that the exact architecture of the NN to be used is generally not known in advance.

Furthermore, some scholars have used other algorithms to study the fault diagnosis of power inverters, such as fuzzy approaches (Li et al., 2006; Zidani et al., 2008; Zhang et al., 2009), and neuro-fuzzy approaches (Awadallah and Morcos, 2003; Park et al., 2004). A fuzzy approach does not require mathematical models of power inverters and only depends on the relationship between input and output to set up a fault diag-

Paper submitted 04/08/15; revised 12/08/15; accepted 06/04/16. Author for correspondence: Kuei-Hsiang Chao (e-mail: chaokh@ncut.edu.tw).
Department of Electrical Engineering, National Chin-Yi University of Technology, Taichung, Taiwan, R.O.C.

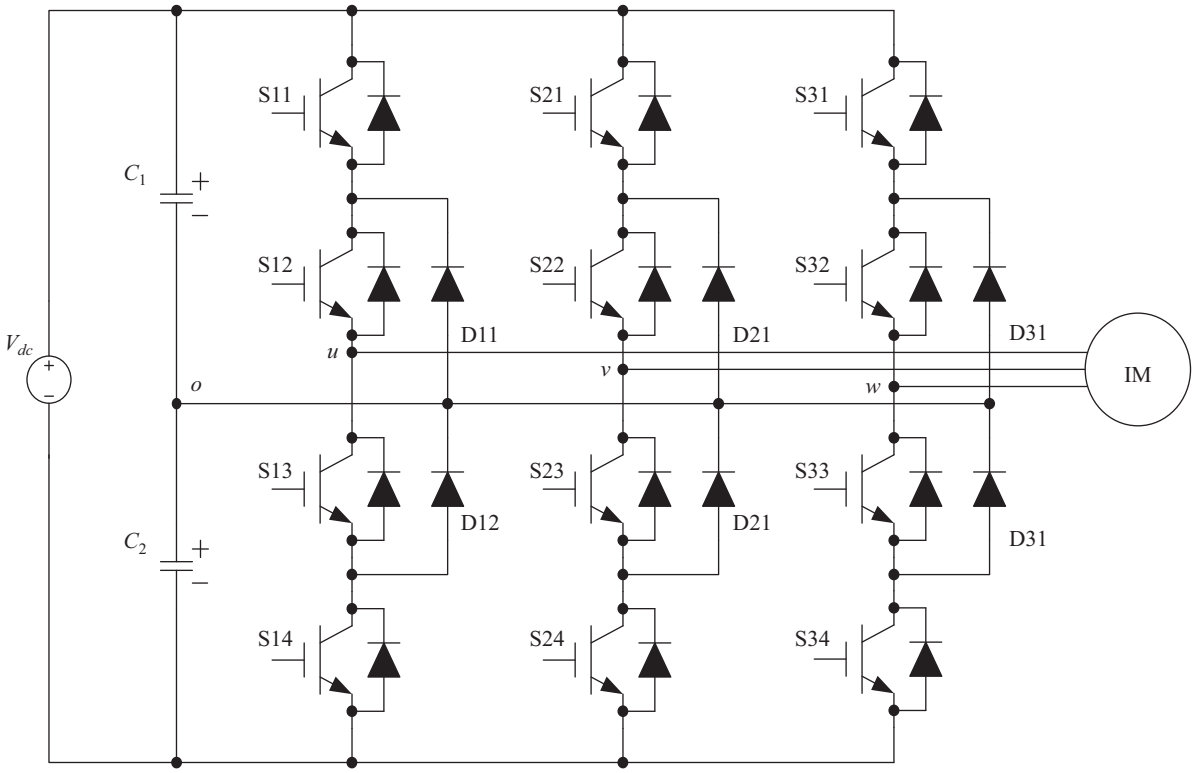

Fig. 1. Structure of the three-level neutral point clamped inverter.

nosis system. However, these algorithms require a lot of time to find the optimal solution. To overcome these problems, it is necessary to combine the features of NNs and fuzzy techniques, which can be accomplished using a neuro-fuzzy approach (Awadallah and Morcos, 2003; Park et al., 2004). In this way, it is possible to develop a fuzzy system embedded in an adaptive NN, without the extra effort needed to build and tune the membership function and the rule parameters. However, in this case, the links only indicate the flow direction of signals between nodes and weights are associated with the links. During the learning process the updating quantities are the parameters of the adaptive nodes.

Consequently, we devise a fault diagnosis method based on a modified neural network to locate the faults of the power transistors in a three-level NPC inverter. The proposed fault diagnosis method has the advantages of less constructed data and a simple learning procedure, such that it can speed up the fault diagnosis response and be implemented easily.

II. FAULT CHARACTERISTICS OF A THREE-LEVEL INVERTER IN A MOTOR DRIVE SYSTEM

Among various structures of inverters (Nabae et al., 1981; Sheng and Fang, 1996; Lai and Shyu, 2002; Corzine et al., 2004; Xiaomin et al., 2004), the neutral point clamped inverter studied by Nabae (Nabae et al., 1981), is the simplest and easiest to control. Therefore, in this study we use a three-level NPC inverter, as represented in Fig. 1, to conduct fault simulation, and create a simulated environment with the circuit simulation software, PSIM. In Fig. 1, the inverter in the motor drive system faces degeneration or spoilage of the devices after being used for a period of time, and these problems can easily result in a faulty motor drive system. Generally speaking, there are three types of power transistor faults in an inverter: short-circuit faults, open-circuit faults and trigger signal faults. Among of these, short-circuit faults result from a voltage overload at two connective points of a switch, which exceeds the rated voltage of the switch and punctures the power transistors. Open-circuit faults result from the lack of triggering signals because the drive circuit fails to generate normal pulse waves and send them to the corresponding switch. Because of this failure, the switch is unable to function normally. Consequently, we establish a simulated environment for a neutral point clamped inverter with PSIM software and study the breakdown of any switches during a designated period of time. By analyzing the simulation, we can observe that the measured waveforms turn to three phase balancing when the inverter is in a normal state. For instance, when an inverter works at the frequency of 60 Hz without the breakdown of any power semiconductor, we can obtain the output waveform of each phase voltage and its corresponding spectrum, as presented in Fig. 2 and Fig. 3.

In Fig. 2, we see that the waveforms of each phase voltage are identical in amplitude and shape. Furthermore, the difference in phase angle between each two waveforms is 120°.

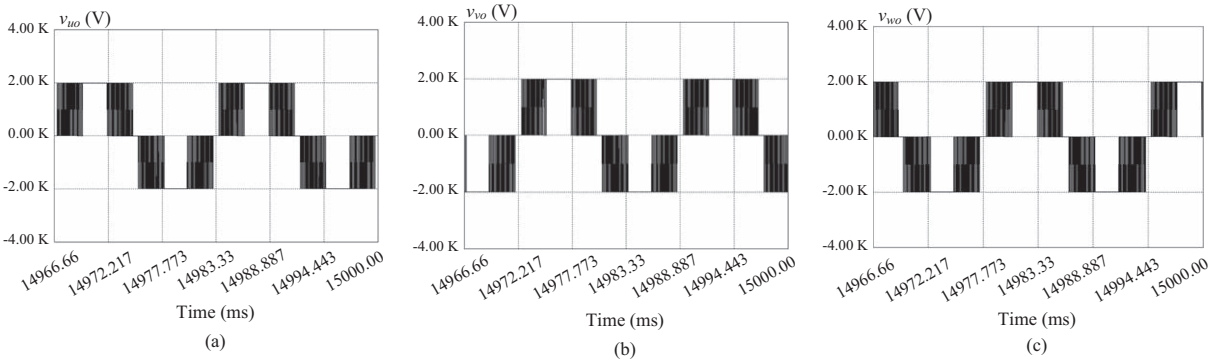

Fig. 2. When the inverter operates at the frequency of 60 Hz, and the power transistors have no faults, the waveforms of the output phase voltage include: (a) phase voltage v_{uo}; (b) phase voltage v_{vo}; (c) phase voltage v_{wo}.

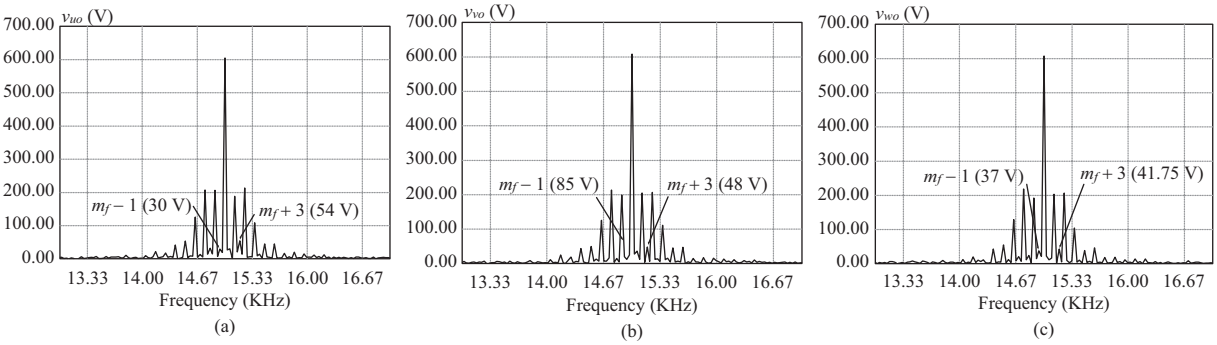

Fig. 3. When the inverter operates at the frequency of 60 Hz, and the power transistors have no faults, the spectrums of the output phase voltage include: (a) phase voltage v_{uo}; (b) phase voltage v_{vo}; (c) phase voltage v_{wo}.

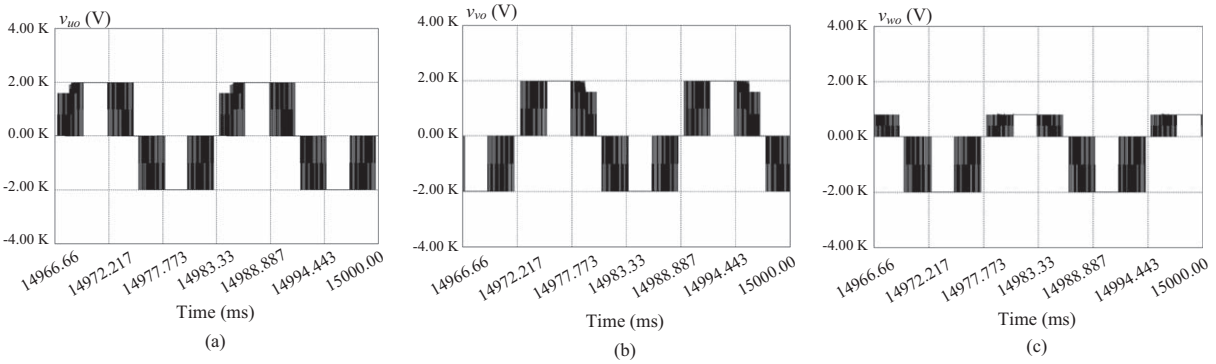

Fig. 4. When the inverter operates at the frequency of 60 Hz, and the power transistor, S33, has a fault, the waveforms of the output phase voltage include: (a) phase voltage v_{uo}; (b) phase voltage v_{vo}; (c) phase voltage v_{wo}.

In addition, once any power transistor in an inverter fails to work, some properties are adjusted. For example, if we cause the power transistor S33 in the scheme of an inverter to break down, we obtain waveforms of each phase voltage in the inverter, as represented in Fig. 4.

Fig. 4 shows that all of the phase voltage waveforms are affected, especially the waveform of the phase voltage v_{wo} of the *w*-leg, which is influenced the most. We can obtain the spectrum of each phase voltage as presented in Fig. 5. Comparing this spectrum with that in Fig. 3, it clearly shows a characteristic spectrum indicating a fault in the power transistor. In this study, we selected the spectrums of $(m_f - 1)$ and $(m_f + 3)$ as the characteristic spectrums, and m_f is defined as the frequency modulation index, whose mathematical form can be written as:

$$m_f \overset{\Delta}{=} \frac{f_{carrier}}{f_{reference}} = \frac{f_{tri}}{f_{sin}} \tag{1}$$

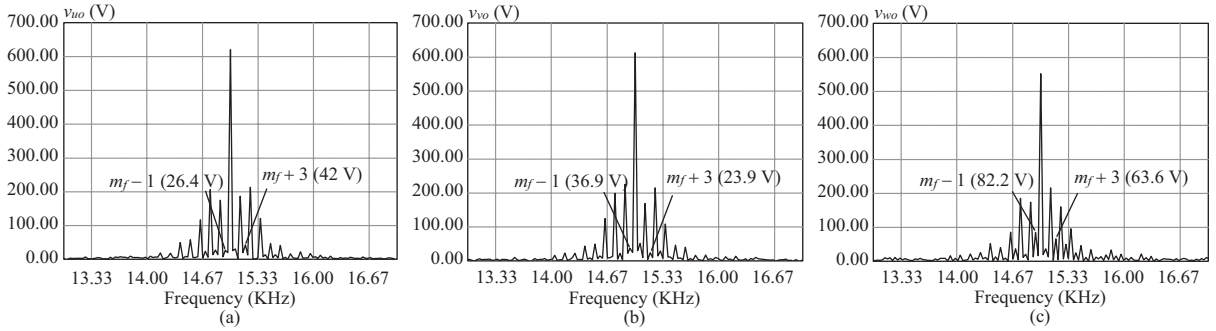

Fig. 5. When the inverter operates at the frequency of 60 Hz, and the power transistor, S33, has a fault, the spectrum of each phase voltage include: (a) phase voltage v_{uo}; (b) phase voltage v_{vo}; (c) phase voltage v_{wo}.

III. FAULT DIAGNOSIS OF THE INVERTER WITH AN EXTENSION NEURAL NETWORK

This study applies the extension neural network (ENN) algorithm for the fault diagnosis of an inverter. This theory contains the calculation of the extension distance of the extension theory and the ability to calculate parallel neural networks. It also has the properties of learning, recalling and generalizing, so this theory is suitable to recognize the properties of objects.

1. Summary of Extension Theory

Extension theory was first proposed in 1983 by Cai (1983). This theory is a formalized tool that is used to consider into problems and solve them by setting the quality and the quantity. The major structure of this theory is comprised of the matter-element theory and extension mathematics. Therefore, extension theory sets up the matter-element model of objects and uses the transforming characteristics as the transformation between the quality and quantity of matter. A matter-element, represented here as "*R*", is the basic element that delineates an object in extension theory. Since "*R*" is composed of the *N* (name), *c* (characteristic) and the corresponding *v* (value) of the offered object, the mathematical form of the matter is as follows (Cai, 1983):

$$R = (N, c, v) \tag{2}$$

In addition, in extension theory, if one matter-element has numerous traits, we can use $c_1, c_2, \ldots, c_m$ to represent each trait and $v_1, v_2, \ldots, v_m$ to represent their corresponding values. The mathematical form representing their mutual relationship is as follows:

$$\mathbf{R} = \begin{bmatrix} N, & c_1, & v_1 \\ & c_2, & v_2 \\ & \cdots & \cdots \\ & c_m, & v_m \end{bmatrix} = \begin{bmatrix} \mathbf{R}_1 \\ \mathbf{R}_2 \\ \cdots \\ \mathbf{R}_m \end{bmatrix} \tag{3}$$

From (3), we name ***R*** as the m-dimensioned matter-element, and use $R_k = (N, c_k, v_k)$ ($k = 1, 2, \ldots, m$) to represent the dimension of each matter element. Consequently, we can rewrite (3) as $\boldsymbol{R} = (\boldsymbol{N, C, V})$, matrix $\boldsymbol{C} = [c_1, c_2, \ldots, c_m]^T$ and matrix = $[v_1, v_2, \ldots, v_m]^T$. In this way, we can describe any object in real life in the form of a multi-dimensional matter element. For example, the inverter in the motor drive system is a DC/AC converter. If we use the extension-element form to represent the measured value of the object, we obtain the mathematical form as follows:

$$R = \begin{bmatrix} \text{Converter}, & \textit{Voltage}, & 110\ \text{V} \\ & \textit{Current}, & 0.5\ \text{A} \\ & \textit{Frequency}, & 60\ \text{Hz} \end{bmatrix} \tag{4}$$

The distance between a range and one point on the real domain in the extension set is defined as follows:

If we assume that *a* is one point in the real field of $(-\infty \sim +\infty)$, and any range $A_1 = \langle va_1, va_2 \rangle$ also belongs to the real field, then the distance between *a* and A_1 can be represented in (5).

$$\psi(a, A_1) = \left| a - \frac{va_1 + va_2}{2} \right| - \frac{va_2 - va_1}{2} \tag{5}$$

2. Extension Neural Network

Fig. 6 shows the structure of the proposed extension neural network, including the input layer, the layer of calculation and the output layer. The process of the structure is to send characteristic samples into the input layer, and to generate the images corresponding to the characteristic sample after setting the weighting parameter range of the layer of the calculation (Chao et al., 2009; Wang et al., 2010). In the calculation layer of this structure, the weighting value w_{gm}^H is the maximum value of the classical region of the *m-th* input characteristic, which belongs to the *g-th* fault category; and w_{gm}^L is the minimum of the classical region of the *m-th* input characteristic, which belongs to the *g-th* fault category. Furthermore, we can observe from the output node in Fig. 6 that whenever one characteristic sample is added into the structure, only one

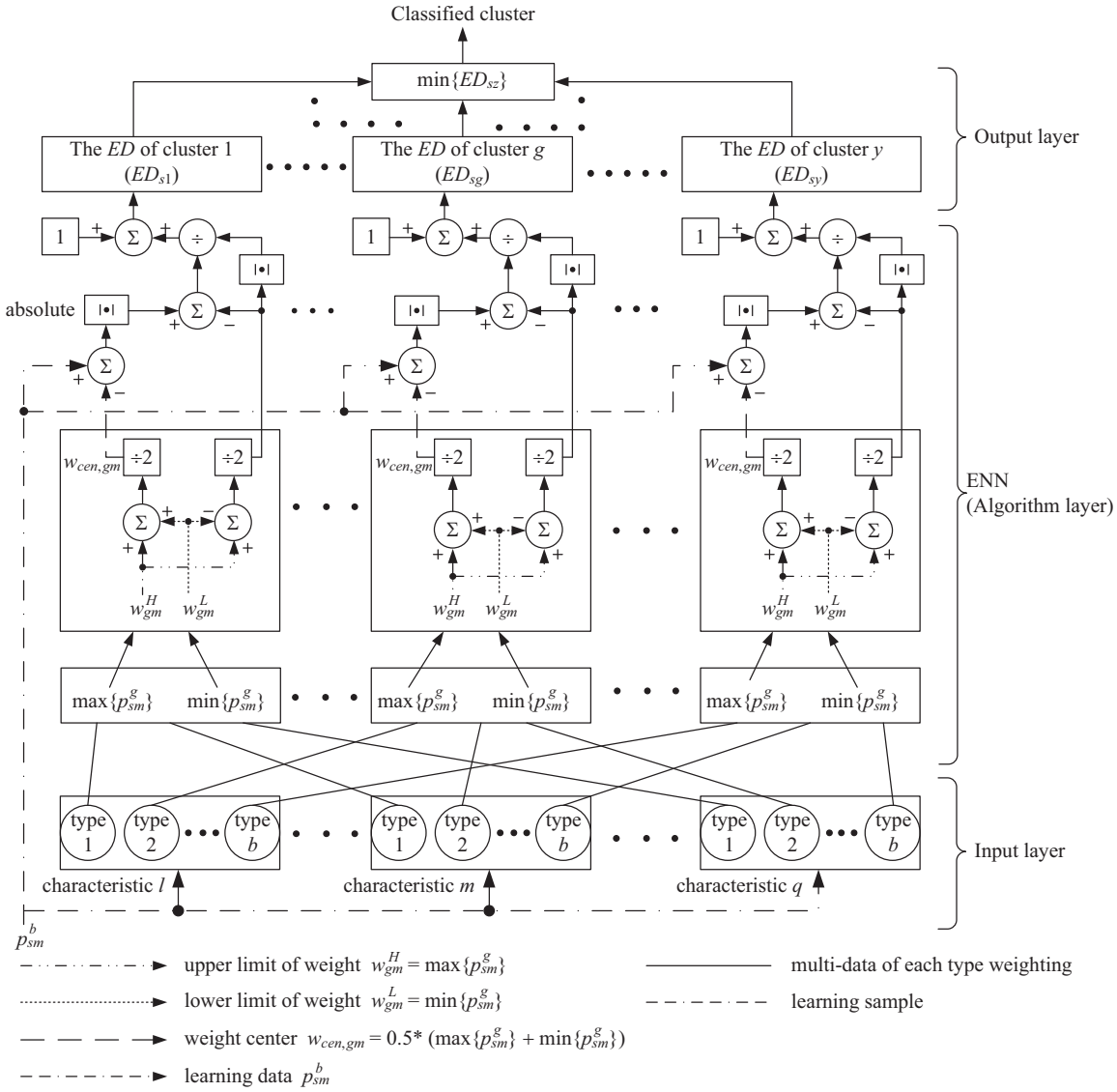

Fig. 6. Proposed scheme of the extension neural network.

output node is altered. If the acquired result is unexpected, we adjust the original weighting value and learn about it until we obtain the demanded goal value. In addition, calculation models of extension neural networks can be divided into two kinds: learning models and calculating models. First, a description of the calculating process for the supervised learning of the extension neural network is given as follows:

Step 1. By the matter-element model of the extension theory, we set the weighting value of linking the input node and the output node as:

$$R_g = \begin{bmatrix} N_g, & c_1, & V_{g1} \\ & c_2, & V_{g2} \\ & \cdots & \cdots \\ & c_m, & V_{gm} \end{bmatrix}, m = 1, 2, \ldots, q;\ g = 1, 2, \ldots, y \quad (6)$$

In (6), C_m represents the *m-th* characteristic in the N_g category, and $V_{gm} = < w_{gm}^L,\ w_{gm}^H >$ is the classical field of the *m-th* characteristic of cluster *g*, and *y* is the total number of classified clusters at the end of output.

This study sets the classical field as the range of the measured value corresponding with the fault characteristics. Herein, the range of the classical field of the extension neural network can be acquired through the following mathematical form:

$$w_{gm}^H = \max_{s \in N_s} \{p_{sm}^g\} \quad (7)$$

$$w_{gm}^L = \min_{s \in N_s} \{p_{sm}^g\} \quad (8)$$

where p_{sm}^g stands for the learning data of the input node of the

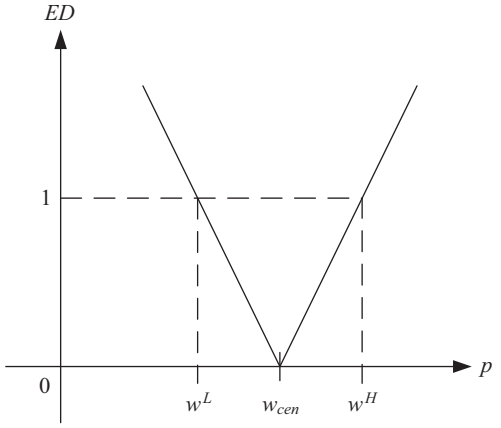

Fig. 7. Extension distance diagram.

extension neural network.

Step 2. The central values of each cluster are calculated and the values are represented as $w_{cen,g}$, and then the mathematic form can be represented as follows:

$$w_{cen,g} = \{w_{cen,g1}, w_{cen,g2}, \ldots, w_{cen,gm}, \ldots\} \tag{9}$$

$$w_{cen,gm} = \frac{(w_{gm}^H + w_{gm}^L)}{2} \tag{10}$$

$$g = 1, 2, \ldots, y;\ m = 1, 2, \ldots, q \tag{11}$$

The first central value of the property in cluster g is represented as $w_{cen,g1}$.

Step 3. Take learning sample s in the category labeled b, and represent it as follows:

$$P_s^b = \{p_{s1}^b, p_{s2}^b, \ldots, p_{sq}^b\},\ b \in y \tag{12}$$

In the above form, y is the number of all kinds of categories.

Step 4. To use the extension distance, as represented in (13), the distance between the learning sample and each cluster can be acquired through the following mathematical form:

$$ED_{sg} = \sum_{m=1}^{q}\left[\frac{\left|p_{sm}^b - w_{cen,gm}\right| - (w_{gm}^H - w_{gm}^L)/2}{\left|(w_{gm}^H - w_{gm}^L)/2\right|} + 1\right] \tag{13}$$

where p_{sm}^b represents the category labeled b and learning sample s with the characteristic of m; $w_{cen,gm}$ is the central weighting value between the *m-th* input node and the *g-th* output node. Fig. 7 represents the extension distance and describes the distance between point p and region $<w^L, w^H>$.

In addition, from Fig. 7, it is apparent that when the range of the region $<w^L, w^H>$ changes, the property of sensibility changes the extension distance as well. Generally speaking, when the classical region of a characteristic becomes larger, it means that the required data are vaguer. This will result in an extension distance with lower sensibility; on the contrary, if we narrow down the classical region of a characteristic, the required data will be more precise and will increase flexibility in the application of the extension distance.

Step 5. After calculation, we can obtain the new cluster g* to which the learning data belongs, and $ED_{sg^*} = \min\{ED_{sg}\}$. If g* = b, we can move directly to step 7; otherwise, we move on to step 6.

Step 6. Adjust and update the weighting value of cluster *b-th* and *g*-th*:

(1) Update the central weighting value of cluster b-th and cluster *g*-th*

$$w_{cen,bm}^{new} = w_{cen,bm}^{old} + \eta(p_{sm}^b - w_{cen,bm}^{old}) \tag{14}$$

$$w_{cen,g^*m}^{new} = w_{cen,g^*m}^{old} - \eta(p_{sm}^b - w_{cen,g^*m}^{old}) \tag{15}$$

(2) Update the weighting values of cluster *b-th* and cluster *g*-th* as

$$\begin{cases} w_{bm}^{H(\text{new})} = w_{bm}^{H(\text{old})} + \eta(p_{sm}^b - w_{cen,\,bm}^{\text{old}}) \\ w_{bm}^{L(\text{new})} = w_{bm}^{L(\text{old})} + \eta(p_{sm}^b - w_{cen,\,bm}^{\text{old}}) \end{cases} \tag{16}$$

$$\begin{cases} w_{g^*m}^{H(\text{new})} = w_{g^*m}^{H(\text{old})} - \eta(p_{sm}^b - w_{cen,\,g^*m}^{\text{old}}) \\ w_{g^*m}^{L(\text{new})} = w_{g^*m}^{L(\text{old})} - \eta(p_{sm}^b - w_{cen,\,g^*m}^{\text{old}}) \end{cases} \tag{17}$$

In (14) to (17), each variable represents different meanings as follows:

η: learning rate of the extension neural network.

$w_{cen,bm}^{new}$: new central weighting value of the *m-th* characteristic of the category labeled b (after learning).

$w_{cen,bm}^{old}$: old central weighting value of the *m-th* characteristic of the category labeled b (before learning).

w_{cen,g^*m}^{new}: new central weighting value of the *m-th* characteristic of the category labeled *g** (after learning).

w_{cen,g^*m}^{old}: old central weighting value of the *m-th* characteristic of the category labeled *g** (before learning).

$w_{bm}^{H(\text{new})}$, $w_{bm}^{L(\text{new})}$: new maximum and minimum weighting value of the *m-th* characteristic of the category labeled b.

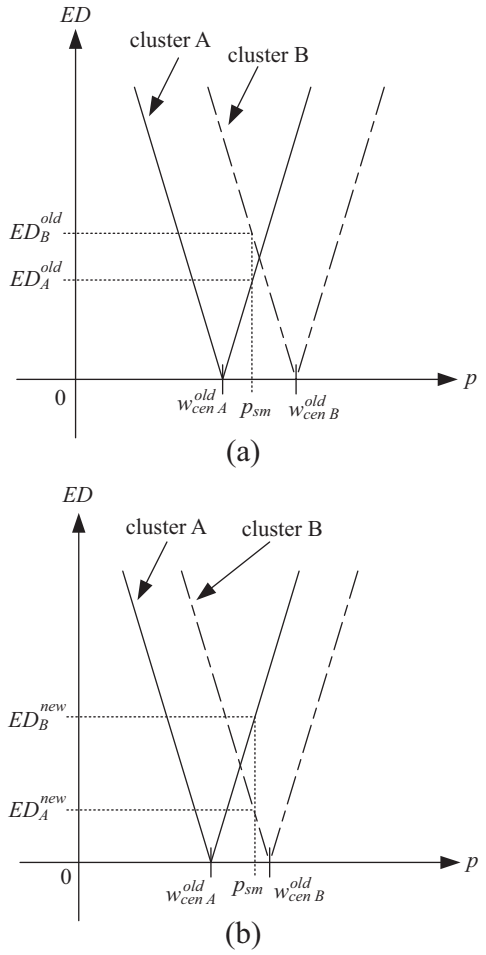

Fig. 8. Adjustment procedure of weight for clusters: (a) before adjusting; (b) after adjusting.

$w_{bm}^{H(\text{old})}$, $w_{bm}^{L(\text{old})}$: old maximum and minimum weighting value of the *m-th* characteristic of the category labeled *b*.

$w_{g^*m}^{H(\text{new})}$, $w_{g^*m}^{L(\text{new})}$: new maximum and minimum weighting value of the *m-th* characteristic of the category labeled *g**.

$w_{g^*m}^{H(\text{old})}$, $w_{g^*m}^{L(\text{old})}$: old maximum and minimum weighting value of the *m-th* characteristic of the category labeled *g**.

The process of adjusting the weighting value in step 6 can be represented and explained as in Fig. 8. In Fig. 8(a), the learning sample p_{sm} should belong to cluster B; but because we get the result, $ED_A^{old} < ED_B^{old}$, after calculation using the extension distance, the sample p_{sm} is classified into cluster A. However, after adjusting the weighting value, the new extension distance will be $ED_A^{new} > ED_B^{new}$, as shown in Fig. 8(b), and so we know that this sample is classified into cluster B. In addition, during the learning process of the weighting value in step 6, we only carry out the adjustment on cluster *b* and cluster *g**, and the weighting value of the other clusters will not be influenced. Therefore, compared with artificial intelligence (AI), which supervises learning, the extension neural network has faster calculation and greater adaptability. In other words, when a new sample is put in, we can find the corresponding output value immediately.

Step 7. Repeat the calculation process from step 3 to step 6 until all the samples are classified. At this point, one epoch is completed.

Step 8. After the process of the classification of all clusters has achieved the state of convergence, or the total difference rate E_r reaches the goal value, then we stop the entire calculation process. If the process mentioned is not finished, then we return to step 3.

The characteristic database this paper adopts is the spectrum of phase voltage with amplitude of the $(m_f - 1)th$ and $(m_f + 3)th$ order harmonics. As $m_f \overset{\Delta}{=} \dfrac{f_{carrier}}{f_{reference}} = \dfrac{f_{tri}}{f_{sin}}$ has been defined, the actual frequency difference between $(m_f - 1)$ and $(m_f + 3)$ is $4f_{tri}/f_{sin}$. In addition, the frequency of f_{tri} is 15 kHz while f_{sin} is 30~90 Hz. Therefore, $(m_f - 1)$ and $(m_f + 3)$ order harmonics are not close database, and thus there will be no error of judgment.

After the extension neural network completes the learning process, we can use the new data to carry out recognition and classification of cluster categories. The process of recognition is explained as follows:

Step 1. Input the weighting matrix of ENN.

Step 2. Calculate the initial central weighting values of different clusters.

Step 3. Read the samples that are waiting to be tested.

$$P_t = \{p_{t1}, p_{t2}, \ldots, p_{tq}\} \tag{18}$$

Step 4. Use (13) to calculate the extension distance between the tested sample and the cluster after learning.

Step 5. Find cluster *g** so as to make $ED_{sg^*} = \min\{ED_{sg}\}$; moreover, set the node value of the corresponding output as 1 in order to judge which cluster category the tested samples belong to.

Step 6. After all the tested samples are classified, the calculation process should be stopped; otherwise, go back to step 3.

IV. SIMULATION RESULTS

The fault spectrum analysis of the above mentioned inverter shows that the fault category of an inverter must be relevant to the characteristics of its breakdown. Therefore, we can illustrate this relationship during the breakdown as follows:

Table 1. Recognition results with different neural networks.

Algorithm	Structure	Learning epochs	Learning accuracy	Recognized accuracy
MLP	6-9-13	1500	92.5%	84.6%
ENN	6-13	3	100%	98.5%

Table 2. Characteristic spectrum data occurring when the inverter operates at 35 Hz and the different power transistors have faults.

No. (fault type)	v_{uo}		v_{vo}		v_{wo}	
	FI_1	FI_2	FI_3	FI_4	FI_5	FI_6
1(F_0)	31.9505	-12.0975	21.6495	-2.1105	39.972	-11.602
2(F_1)	128.2825	30.3175	51.452	21.322	32.3105	3.0875
3(F_2)	65.3005	10.3695	53.561	32.678	29.0965	11.2215
4(F_3)	92.921	-25.199	48.003	16.156	11.5915	1.1155
5(F_4)	217.635	-27.555	44.996	27.703	29.3865	4.6405
6(F_5)	29.1504	-22.6296	123.2865	30.1035	45.2555	-1.1985
7(F_6)	21.223	-5.085	46.1405	3.0265	40.281	4.489
8(F_7)	25.344	12.326	105.141	-9.489	25.5835	-0.3085
9(F_8)	24.281	-9.48	211.23	-33.45	34.9285	4.3335
10(F_9)	67.633	-1.623	22.8235	-4.0175	120.3305	26.7295
11(F_{10})	51.814	-7.236	28.039	4.02	53.3175	9.5665
12(F_{11})	45.7845	-1.4975	32.1795	10.4135	94.318	-24.242
13(F_{12})	61.81	16.158	32.7155	7.7545	238.095	-3.555

$$R = (N, c, v) = (F_n, FI_n, v) \tag{19}$$

Here, R is the fault matter-element of the inverter; N represents the fault category of the inverter, as represented by F_n (n = 0, 1, …); c is the characteristic of the fault and is represented by the symbol FI_n (n = 1, 2, …); v is the measured value corresponding with the characterisitics of the fault. To explore inverter faults, this study conducts simulation analysis under two conditions: the power transistors have no breakdowns and each of the twelve power transistors (S11~S34) have breakdowns; therefore, we use the following symbols to represent the thirteen fault categories:

F_0: No power transistor breaks down.
F_1: Power transistor S11 breaks down.
F_2: Power transistor S12 breaks down.
F_3: Power transistor S13 breaks down.
F_4: Power transistor S14 breaks down.
F_5: Power transistor S21 breaks down.
F_6: Power transistor S22 breaks down.
F_7: Power transistor S23 breaks down.
F_8: Power transistor S24 breaks down.
F_9: Power transistor S31 breaks down.
F_{10}: Power transistor S32 breaks down.
F_{11}: Power transistor S33 breaks down.
F_{12}: Power transistor S34 breaks down.

Therefore, the characteristics of the breakdowns can be represented as follows:

FI_1 and FI_2: The characteristic spectrum of the phase voltage, v_{uo}, of u leg,
FI_3 and FI_4: The characteristic spectrum of the phase voltage, v_{vo}, of v leg,
FI_5 and FI_6: The characteristic spectrum of the phase voltage, v_{wo}, of w leg.

The proposed fault diagnosis system of the three-level inverter simulates the breakdown of each power transistor by using PSIM software with the inverter's range of operation frequency set from 30~90 Hz. Moreover, to enhance the judging sensitivity of characteristic spectrum, the two characteristic spectrums are dealt with individually in (20) and (21) so as to serve as the characteristics of the inverter's fault category.

$$FI_1 = FI_3 = FI_5 = 0.5\,[(m_f - 1) + (m_f + 3)] \tag{20}$$

$$FI_2 = FI_4 = FI_6 = 0.5\,[(m_f - 1) - (m_f + 3)] \tag{21}$$

This study uses 25 different frequencies and the characteristic values of the spectrum under different power transistor faults in a NPC inverter. There is a total 325 samples. This data can act as the learning data of the proposed extension neural network (ENN) and multilayer perceptions (MLP) to establish a fault diagnosis system for the three-level NPC inverter. To prove the effectiveness of the proposed fault diagnosis system, the measured power transistor breakdown data acquired through the simulation amounts to 468. These data can be tested for different neural networks based on the fault diagnosis system. Table 1 shows the recognition results with different neural networks, in which we use 325 samples to

Table 3. Characteristic spectrum data occurring when the inverter operates at 55 Hz and the different power transistors have faults.

No. (fault type)	v_{uo}		v_{vo}		v_{wo}	
	FI_1	FI_2	FI_3	FI_4	FI_5	FI_6
1(F_0)	31.092	-10.45	22.27	-0.325	39.0325	-12.3885
2(F_1)	126.425	27.815	50.4235	28.4715	25.433	2.285
3(F_2)	63.303	7.444	49.3835	13.3525	22.5176	-18.9234
4(F_3)	94.1235	-29.3665	44.8165	9.0195	18.1945	3.5745
5(F_4)	213.34	-33.38	54.344	14.742	24.6125	-6.0005
6(F_5)	32.1765	-15.8635	122.115	35.025	41.9275	-5.1325
7(F_6)	30.5045	-13.4255	53.281	12.181	39.8965	-6.1325
8($F_{7)}$	41.629	23.246	111.42	8.1	31.6575	5.7855
9(F_8)	19.1325	-2.1475	210.71	-21.19	40.737	-1.13
10(F_9)	56.455	-5.423	27.877	0.285	115.3045	34.0455
11(F_{10})	55.224	-3.292	27.3905	1.5715	51.108	4.707
12(F_{11})	35.315	-14.624	37.721	27.09	91.836	-26.064
13(F_{12})	53.5185	0.9745	31.8005	8.4885	225.1	-14.92

Table 4. Characteristic spectrum data occurring when the inverter operates at 75 Hz and the different power transistors have faults.

No. (fault type)	v_{uo}		v_{vo}		v_{wo}	
	FI_1	FI_2	FI_3	FI_4	FI_5	FI_6
1(F_0)	49.2365	-21.8755	42.9155	-16.1005	48.3415	-20.1435
2(F_1)	115.059	34.771	53.445	19.875	25.29545	-19.9996
3(F_2)	54.6545	9.7115	55.394	18.353	20.49187	-19.5611
4(F_3)	100.2245	-0.7955	41.7895	20.4305	28.36555	19.46645
5(F_4)	214.785	-29.055	54.0535	16.4685	26.8615	-0.8835
6(F_5)	29.687	-15.737	115.5115	27.8385	45.606	-6.586
7(F_6)	28.9875	-12.147	46.1425	9.613	44.301	-5.3694
8($F_{7)}$	43.0355	22.8935	113.125	6.245	30.5475	7.8555
9(F_8)	27.547	-7.456	204.04	-30.8	41.586	0.272
10(F_9)	51.871	-6.243	32.906	1.149	107.0905	34.0495
11(F_{10})	51.846	-4.238	29.837	3.313	43.7365	9.8275
12(F_{11})	34.9945	-3.5265	42.9964	34.5916	96.1075	-11.7825
13(F_{12})	47.27	-0.241	34.6615	11.0375	224.815	-16.345

learn and 468 samples for testing. From this table, it is evident that the proposed extension neural network has a shorter learning time, greater learning capacity and a better recognized accuracy rate than the multilayer perceptions approach.

Moreover, Tables 2, 3 and 4 represent the characteristic spectrums of each phase voltage when each switch breaks down under the operation frequencies of 35 Hz, 55 Hz and 75 Hz. We input the test data from Table 2 to Table 4 to the established fault diagnosis system for the inverter. Then we obtain the recognition results in Table 5 to Table 7. From the tables, we find that each breakdown data can be correctly recognized. For instance, from Table 6, we observe that the second test data, ED_{F1} = 2.82, is the smallest extension distance value, indicating that the power transistor, S11, breaks down (i.e., fault type is F_1). In addition, in the same data, ED_{F8} = 18.005 is the maximum, which represents that when this test data belongs to S24, the breakdown rate is the lowest. The recognition results of other test data can also be analyzed in this way.

Adopting the proposed ENN approach, the frequency spectrum characteristics is in between a range. The range is considered as the upper and lower limit of training weight. Despite the fact that there are noise perturbations, the fault diagnose method of ENN approach still has its robustness.

In order to verify that the proposed approach can also be applied to fault diagnose, while several power semiconductor switches are faulting at the same time, this paper tests on S11 and S33 as an example. Assume that the operation frequency of the inverter is 60 Hz, and that each phase of output voltage

Table 5. Recognition results occurring when the inverter operates at 35 Hz and the different power transistors have faults.

Test No. / ED	1	2	3	4	5	6	7	8	9	10	11	12	13
ED_{F0}	**3.422**	14.788	12.077	9.194	15.427	10.152	6.473	13.043	19.511	14.998	4.969	8.864	21.798
ED_{F1}	11.734	**2.193**	4.930	5.304	9.158	18.082	7.337	15.866	33.294	14.749	9.475	12.113	18.862
ED_{F2}	4.385	6.961	**4.095**	6.833	11.469	8.915	3.190	7.445	15.082	9.508	3.651	5.572	14.752
ED_{F3}	9.054	6.597	4.836	**3.671**	10.135	14.327	7.173	13.712	23.697	12.124	6.424	11.257	19.618
ED_{F4}	14.548	6.948	7.620	5.148	**3.019**	19.241	10.017	19.568	38.739	19.082	12.868	15.893	24.483
ED_{F5}	4.080	11.679	7.842	9.665	14.690	**3.004**	4.412	6.188	6.465	13.108	5.055	7.881	21.352
ED_{F6}	3.910	9.921	7.243	7.772	12.984	6.928	**1.969**	8.056	12.776	12.143	3.389	7.955	20.778
ED_{F7}	7.330	8.879	5.728	9.521	15.395	8.062	5.432	**3.326**	10.879	12.231	6.286	10.400	18.245
ED_{F8}	8.859	17.300	12.305	14.389	19.809	9.388	7.432	8.496	**3.465**	15.370	7.910	14.447	26.697
ED_{F9}	10.259	16.826	9.648	12.562	22.895	15.127	8.757	15.441	20.494	**4.101**	4.960	6.148	12.293
ED_{F10}	5.699	13.154	7.724	10.054	17.433	11.935	4.816	12.461	17.866	9.614	**0.581**	7.359	18.896
ED_{F11}	7.317	14.555	10.529	11.694	18.388	18.255	7.635	18.693	34.609	10.201	6.399	**2.883**	12.701
ED_{F12}	8.815	15.916	9.886	12.115	24.701	17.341	10.176	15.813	26.994	8.541	7.166	4.889	***4.007***
Real fault type	F_0	F_1	F_2	F_3	F_4	F_5	F_6	F_7	F_8	F_9	F_{10}	F_{11}	F_{12}
Recognized fault type	F_0	F_1	F_2	F_3	F_4	F_5	F_6	F_7	F_8	F_9	F_{10}	F_{11}	F_{12}

Table 6. Recognition results occurring when the inverter operates at 55 Hz and the different power transistors have faults.

Test No. / ED	1	2	3	4	5	6	7	8	9	10	11	12	13
ED_{F0}	***3.637***	15.367	9.231	8.713	14.350	10.614	4.905	13.465	18.300	14.044	4.667	9.761	18.993
ED_{F1}	11.453	***2.820***	5.498	5.896	10.192	17.759	7.283	13.734	32.433	14.407	9.128	11.992	19.702
ED_{F2}	4.250	7.414	***3.182***	6.885	11.802	8.324	3.328	6.938	13.446	8.812	3.310	7.102	13.616
ED_{F3}	8.827	6.760	6.051	***3.621***	11.446	14.092	7.116	12.232	24.185	11.960	6.863	11.145	19.200
ED_{F4}	14.428	6.970	8.670	6.026	***2.703***	19.825	7.774	19.767	38.973	17.904	13.226	13.538	23.384
ED_{F5}	3.988	12.114	7.005	10.138	14.530	***2.332***	3.276	6.367	5.713	11.995	5.250	7.283	18.217
ED_{F6}	3.716	10.610	6.667	7.334	13.206	7.243	***2.079***	7.989	12.205	10.829	3.559	8.086	18.913
ED_{F7}	7.107	9.694	6.193	8.905	15.092	7.803	6.438	***2.739***	10.437	11.579	5.783	12.650	18.126
ED_{F8}	8.918	18.005	13.067	13.897	20.372	8.764	8.825	9.466	***3.980***	14.681	8.636	15.685	24.204
ED_{F9}	10.125	17.188	10.480	11.963	23.958	14.870	9.653	13.681	20.452	***2.530***	5.612	8.394	10.763
ED_{F10}	5.595	13.694	8.484	9.245	18.959	11.812	6.177	11.213	17.838	8.122	***1.478***	9.423	16.671
ED_{F11}	7.019	14.608	8.102	11.970	19.801	17.605	7.390	18.507	33.422	8.372	6.790	***2.401***	9.746
ED_{F12}	8.676	15.948	6.716	12.461	23.968	16.423	9.098	15.027	25.530	7.820	6.343	7.741	***1.895***
Real fault type	F_0	F_1	F_2	F_3	F_4	F_5	F_6	F_7	F_8	F_9	F_{10}	F_{11}	F_{12}
Recognized fault type	F_0	F_1	F_2	F_3	F_4	F_5	F_6	F_7	F_8	F_9	F_{10}	F_{11}	F_{12}

Table 7. Recognition results occurring when the inverter operates at 75 Hz and the different power transistors have faults.

Test No. / ED	1	2	3	4	5	6	7	8	9	10	11	12	13
ED_{F0}	***4.241***	15.004	9.990	12.442	14.656	9.312	4.194	13.721	17.756	13.254	5.045	10.030	19.100
ED_{F1}	10.161	***3.550***	6.477	3.746	9.537	16.690	7.487	14.188	31.993	13.353	8.528	10.934	19.501
ED_{F2}	5.223	7.768	***3.677***	4.715	11.341	7.950	3.141	7.201	13.745	7.838	2.749	6.417	13.247
ED_{F3}	9.211	7.606	7.030	***1.934***	10.643	13.450	6.942	12.207	23.501	11.128	5.825	11.080	19.132
ED_{F4}	11.544	8.247	8.714	7.268	***2.098***	18.466	9.407	20.073	37.903	16.538	12.284	13.692	22.811
ED_{F5}	5.934	11.779	6.729	8.619	14.228	***1.815***	3.159	6.650	5.076	10.920	5.095	6.491	17.713
ED_{F6}	5.238	11.610	7.336	7.730	12.510	6.107	***1.304***	8.415	11.562	9.545	3.469	7.776	18.635
ED_{F7}	8.214	10.127	5.872	8.347	14.581	7.396	6.826	***2.756***	10.720	10.698	5.354	11.690	18.146
ED_{F8}	9.752	19.437	13.370	12.535	19.418	8.919	8.935	9.224	***2.621***	13.653	7.512	14.853	23.939
ED_{F9}	10.351	18.366	11.085	9.447	23.199	14.192	8.810	13.623	19.424	***2.093***	5.518	7.294	11.226
ED_{F10}	6.417	15.281	9.006	8.276	18.072	10.984	5.126	11.028	16.633	7.050	***1.585***	8.954	17.343
ED_{F11}	7.384	13.599	8.420	10.123	19.583	16.026	6.352	19.121	32.449	6.893	6.681	***3.349***	8.566
ED_{F12}	8.790	14.657	7.128	11.844	24.243	15.440	8.640	15.329	25.226	7.822	7.039	6.442	***2.313***
Real fault type	F_0	F_1	F_2	F_3	F_4	F_5	F_6	F_7	F_8	F_9	F_{10}	F_{11}	F_{12}
Recognized fault type	F_0	F_1	F_2	F_3	F_4	F_5	F_6	F_7	F_8	F_9	F_{10}	F_{11}	F_{12}

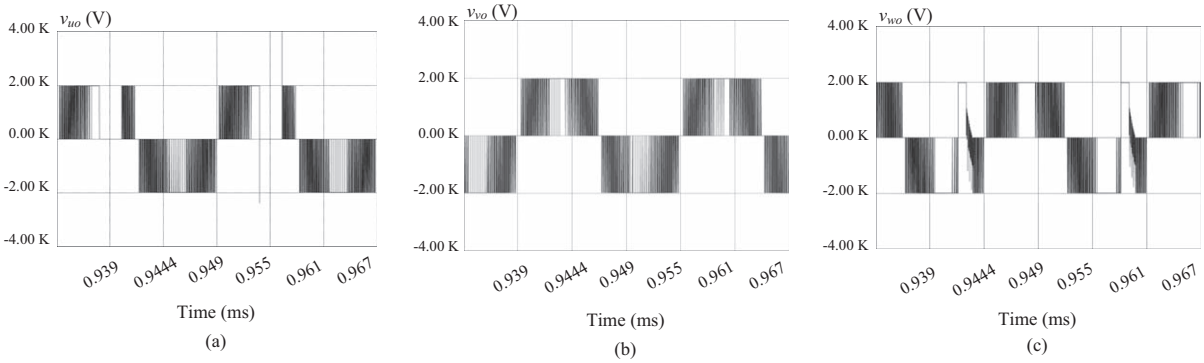

Fig. 9. When the inverter operates at the frequency of 60 Hz, and the power transistors, S11 and S33, have a fault, the waveforms of the output phase voltage include: (a) phase voltage v_{uo}; (b) phase voltage v_{vo}; (c) phase voltage v_{wo}.

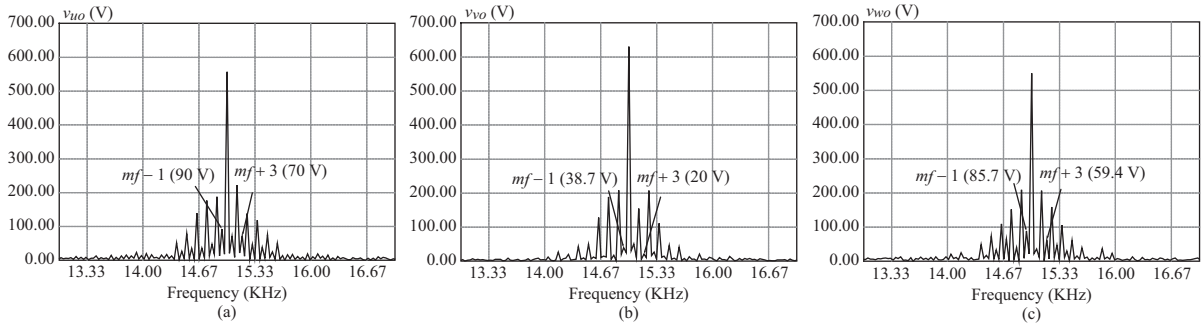

Fig. 10. When the inverter operates at the frequency of 60 Hz, and the power transistors, S11 and S33, have a fault, the spectrum of each phase voltage include: (a) phase voltage v_{uo}; (b) phase voltage v_{vo}; (c) phase voltage v_{wo}.

waves of faults while switches S11 and S33 are fault is shown in Fig. 9. It can observe that when the fault of switches occurs in *u*-leg and *w*-leg, the phase voltage v_{u0} and v_{w0} will be abnormal, causing three-phase unbalance of output voltage. The frequency spectrum of each phase voltage is shown in Fig. 10. Comparing Fig. 5 and Fig. 10, it can be found that the spec-

trum amplitude of the $(m_f - 1)th$ and $(m_f + 3)th$ order harmonics in v_{v0} and v_{w0} has little change. However, the spectrum amplitude of $(m_f - 1)th$ and $(m_f + 3)th$ order harmonic increases in v_{u0} due to the fault of S11 switch in u -leg. From this, when multiple switch faults occur, diagnosing faults through ENN produces close minimal values of many multiple extension distance. These close minimal values which belong to fault type can diagnose the position of multiple switches.

V. CONCLUSIONS

The extension neural network algorithm adopted in this study includes the extension matter-element model and neural network theory. This algorithm has the ability to supervise learning and recall and generalize the neural network. Therefore, it is suitable for the fault diagnosis of an inverter used in marine vessels. For the fault diagnosis of the three-level inverter, we establish a three-level neutral point clamped DC/AC inverter with the circuit-simulated software, PSIM. When the inverter starts to simulate the breakdown (we assume that at each moment only one power transistor breaks down), then we obtain thirteen fault categories, which include the no-fault category and the types of breakdowns of each of the twelve power transistors. Analysis of the simulation shows that only when the inverter breaks down does a characteristic spectrum occur during the breakdown. Therefore, we can use the extension neural network to establish an artificial fault diagnosis system for the three-level NPC inverter. Finally, to verify the feasibility of the proposed artificial fault diagnosis system, we tested the test data. The results of the tests show that the fault categories of the three-level NPC inverter can be correctly diagnosed and classified.

ACKNOWLEDGMENTS

This work was supported by the Ministry of Science and Technology, Taiwan, under the Grant MOST 103-2221-E-167-015-MY3.

REFERENCES

Awadallah, M. A. and M. M. Morcos (2003). Diagnosis of switch open-circuit fault in PM brushless DC motor drives. Proceeding of Power Engineering Conference on Large Engineering Systems, 69-73.

Cai, W. (1983). The extension set and incompatibility problem. Journal of Scientific Exploration 1, 81-93.

Chao, K. H., C. J. Li and M. H. Wang (2009). A maximum power point tracking method based on extension neural network for PV systems. Lecture Notes in Computer Science 5551, 745-755.

Corzine, K. A., M. W. Wielebski, F. Z. Peng and J. Wang (2004). Control of cascaded multilevel inverters. IEEE Transactions on Power Electronics 19, 732-738.

Daher, S., J. Schmid and F. L. M. Antunes (2008). Multilevel inverter topologies for stand-alone PV systems. IEEE Transactions on Industrial Electronics 55, 2703-2712.

Ju, Y., M. A. Masrur, Z. H. Chen and B. Zhang (2006). Model-based fault diagnosis in electric drives using machine learning. IEEE/ASME Transactions on Mechatronics 11, 290-303.

Khomfoi, S. and L. M. Tolbert (2007). Fault diagnostic system for a multilevel inverter using a neural network. IEEE Transactions on Power Electronics 22, 1062-1069.

Lai, Y. S. and F. S. Shyu (2002). Topology for hybrid multilevel inverter. IEE Proceedings: Electric Power Applications 149, 449-458.

Li, D. H., X. F. Sun and W. Y. Wu (2006). The studies of single-phase inverter fault diagnosis based on D-S evidential theory and fuzzy logical theory. Proceeding of IEEE Power Electronics Motion Control Conference, 1-4.

Lu, B. and S. K. Sharma (2009). A literature review of IGBT fault diagnostic and protection methods for power inverters. IEEE Transactions on Industrial Applications 45, 724-738.

Nabae, A., I. Takahashi and H. Akagi (1981). A new neutral-point clamped PWM inverter. IEEE Transactions on Industry Applications 17, 518-523.

Park, J. H., D. H. Kim, S. S. Kim, D. J. Lee and M. G. Chun (2004). C-ANFIS based fault diagnosis for voltage-fed PWM motor drive systems. Proceeding of the IEEE Fuzzy Information Conference, 379-383.

Rodríguez, J., J. S. Lai and F. Z. Peng (2002). Multilevel inverters: A survey of topologies, controls, and applications. IEEE Transactions on Industrial Electronics 49, 724-738.

Rodriguez, J. I. and S. B. Leeb (2006). A multilevel inverter topology for inductively coupled power transfer. IEEE Transactions on Power Electronics 21, 1607-1617.

Sheng, L. J. and Z. P. Fang (1996). Multilevel converters - A new breed of power converters. IEEE Transactions on Industry Applications 32, 509-517.

Wang, M. H., K. H. Chao, W. T. Sung and G. J. Huang (2010). Using ENN-1 for fault recognition of automotive engine. Expert System with Applications 37, 2943-2947.

Xiaomin, K., K. A. Corzine and Y. L. Familiant (2004). A unique fault-tolerant design for flying capacitor multilevel inverter. IEEE Transactions on Power Electronics 19, 979-987.

Zhang, K., B. Jiang and M. Staroswiecki (2009). Dynamic output feedback fault tolerant controller design for Takagi-Sugeno fuzzy systems with actuator faults. IEEE Transactions on Fuzzy Systems 18, 194-201.

Zidani, F., D. Diallo, M. E. H. Benbouzid and R. N. Saïd (2008). A fuzzy-based approach for the diagnosis of fault modes in a voltage-fed PWM inverter motor drive. IEEE Transactions on Industrial Electronics 55, 586-593.